

Content from this work may be used under the terms of the CC BY 3.0 licence (© 2018). Any distribution of this work must maintain attribution to the author(s), title of the work, publisher, and DOI.

# X-RAY INVESTIGATION ON THE SUPERCONDUCTING SOURCE FOR IONS (SUSI)\*

Derek Neben<sup>†</sup>, Jesse Fogleman, Bryan Isherwood, Daniela Leitner<sup>1</sup>, Guillaume Machicoane  
 Shane Renteria, Jeffry Stetson, Larry Tobos

National Superconducting Cyclotron Laboratory, Michigan State University, East Lansing, MI, USA

<sup>1</sup> Lawrence Berkeley National Laboratory, Berkeley, CA, USA

## Abstract

Heavy ion facilities such as the National Superconducting Cyclotron Laboratory (NSCL) often use ECR Ion Sources (ECRIS) for the production of highly charged ions to increase the efficiency of accelerating structures. Axial bremsstrahlung emission was studied on the Superconducting Source for Ions (SuSI) at the NSCL for 18 GHz and 13 GHz operation with oxygen. The hot electron temperatures were estimated from the bremsstrahlung high energy tail and seem to depend only on magnetic minimum in the same way as was found on VENUS [1], even in the case where 18 GHz and 13 GHz frequencies were compared for similarly sized ECR zones. Additionally, the time independent x-ray power increased at a significantly larger rate when operating the source in known regions of instability such as where the magnetic minimum approaches the ECR zone [2]. The results are discussed in the context of electron losses due to magnetic confinement.

## INTRODUCTION

We present the bremsstrahlung measurements from a fast sputtering campaign conducted on the Superconducting Source for Ions (SuSI) at the National Superconducting Cyclotron Laboratory (NSCL). The SuSI source is a fully superconducting ECR ion source nominally operating at 18 GHz [3] and 24 GHz [4] microwave frequencies. Following the path set by Geller's scaling laws for ECRIS [5] the plasma density and beam current of ECR ion sources increase with the square of the operating frequency and as proposed more recently [6] with the square of the magnetic field. However, increasing the magnetic field increases the bremsstrahlung emission from the source and stresses the cryostats of 3<sup>rd</sup> generation fully superconducting ion sources. Dynamic heat loads on the order of several watts [7] have been observed as a result of x-rays produced by bremsstrahlung as electrons escape the ECR plasma, in particular when operating with higher magnetic fields. The x-ray investigation presented herein focused on how x-ray temperature changed with magnetic minimum following measurements previously done by the LBNL group using the VENUS source [1].

Bremsstrahlung results are presented for 18 GHz operation up to 400 W applied microwave power and 13 GHz for a microwave power level of 100 W. Continuous Wave (CW)

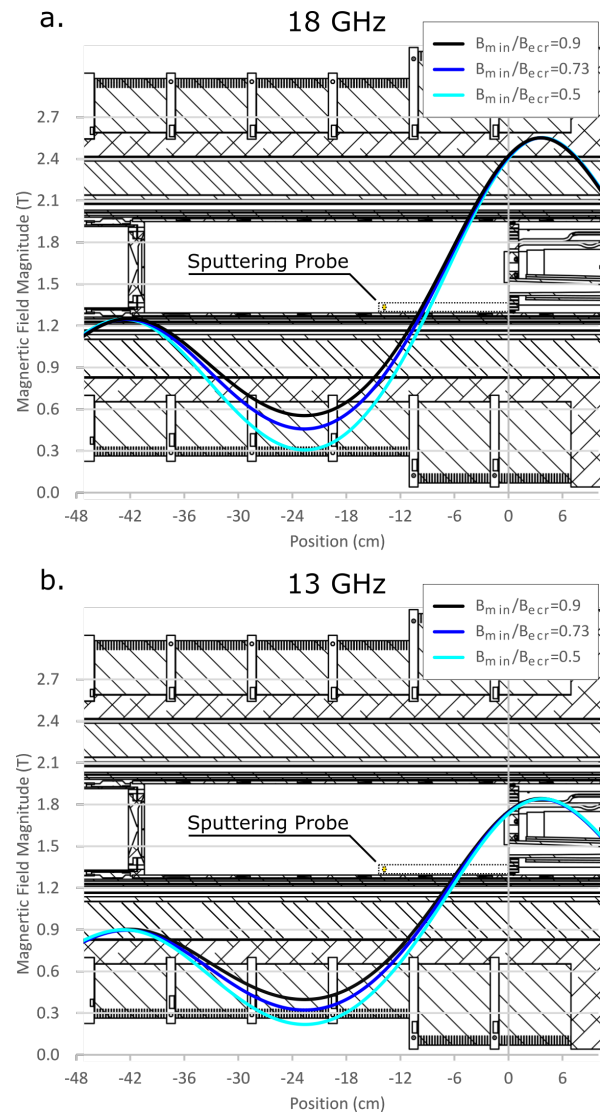


Figure 1: SuSI Magnetic field as simulated using Poisson with the radial sputtering probe developed for SuSI (dotted line). Three field configurations:  $B_{min}/B_{ecr}=0.5$ ,  $0.73$ , and  $0.9$  were selected for both 18 GHz and 13 GHz operation. The magnetic fields were scaled with frequency resulting in the same ECR zone size for constant  $B_{min}/B_{ecr}$  ratio. The radial sputtering probe was inserted in between the electron flutes on the injection baffle along the plasma chamber wall.

\* Work supported by Michigan State University and the National Science Foundation: NSF Award Number PHY-1415462

<sup>†</sup> neben@nsl.msu.edu

Table 1: Characteristics of the Magnetic Field Configurations Used in the Study

Frequency	18 GHz			13 GHz		
	$B_{min}/B_{ecr}$	0.5	0.73	0.9	0.5	0.73
$B_{min}$ (T)	0.31	0.46	0.55	0.22	0.32	0.40
$B_{inj}$ (T)	2.55	2.55	2.55	1.84	1.84	1.84
$B_{ext}$ (T)	1.25	1.25	1.25	0.90	0.90	0.90
$B_{rad}$ (T)	1.25	1.25	1.25	0.93	0.93	0.93
ECR Length (cm)	16.3	12.8	9.3	16.5	13.0	9.3
$B_{ext}/B_{min}$	4.03	2.72	2.27	4.09	2.81	2.25

sputtering Charge State Distributions (CSD) are presented comparing 13 GHz and 18 GHz operation for constant microwave power, magnetic minimum ( $B_{min}$ ), and ECR zone size.

## EXPERIMENTAL SET-UP

An off-axis radial sputter probe developed for SuSI was used with a gold sputter sample for these measurements. Gold currents ranging from 100's of nanoamperes to microamperes were used to avoid saturating the plasma with the heavy metal. Microwave power was limited to 400 W to protect the sputter sample and sputtering probe from damage. The probe consists of a conducting inner core and an insulating outer shield, and to provide the sputter sample access to the plasma a small hole was cut at the end of the insulating shield. The outer insulator was cylindrical in cross section with an outer diameter of 11.4 mm and protruded 14.5 cm from the injection baffle. The probe was passed from the injection flange along the plasma chamber wall (see Fig. 1) in between the electron flutes on the injection baffle.

Table 1 summarizes the parameters explored for the study. We used two microwave frequencies and three mirror configurations for each frequency. The fields for the 13 GHz configurations were scaled by the ratio of the frequencies. For constant frequency, the injection and extraction field strengths were fixed varying the magnetic minimum as can be seen in Fig. 1a-b. A field with constant  $B_{min}/B_{ecr}$  ratio had a similar ECR zone size.

Typical plasma parameters are summarized in Table 2. Oxygen was used as the mixing gas for each plasma studied, and the leak valve set-point remained constant as the magnetic field was changed within a selection of frequency and microwave power. 13 GHz operation was limited to 100 W, since the narrow bandwidths optimized for the 18 GHz transmission line DC break and the microwave window lead to a high reflected power, while up to 400 W was used for 18 GHz operation. The microwave power for  $B_{min}/B_{ecr}=0.9$  (at 18 GHz) had to be limited to 200 W to avoid damaging the probe by the plasma at this field.

Energy resolved x-ray spectra were measured using an axial High Purity Germanium (HPGe) x-ray detector. The HPGe detector was used with an Ortec 671 linear shaper amplifier and Ortec Easy MCA (Multi Channel Analyzer) with pileup rejection to collect the detector signals. This

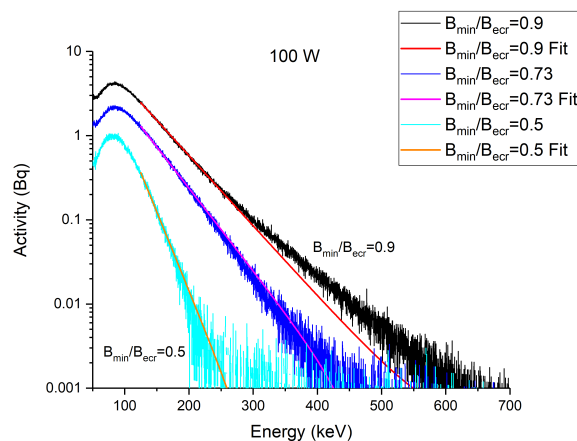


Figure 2: X-ray spectra corrected for detector efficiency and background radiation produced by an oxygen plasma driven at 18 GHz with 100 W microwave power. An exponential decay function was applied to the bremsstrahlung spectra starting at 125 keV through the end of the datafile (1440 keV).

combination of amplifier and MCA with pileup rejection could accept a maximum 20 k counts per second (if uniformly spaced in time), the maximum average count rate observed in the experiment was 2.2 k counts per second and was well within the capabilities of the data acquisition system. The detector was placed at the end of a narrow collimation channel with a tungsten insert similar to the one described in [8]. The collimator allowed an opening angle of about 20 minutes projecting a circle of 13 mm in diameter on the extraction electrode. As the extraction electrode aperture was 8 mm in diameter the observed x-rays were mainly produced by bremsstrahlung from electrons lost from the magnetic trap and striking the extraction electrode. The HPGe detection efficiency was measured off-line using a  $^{152}\text{Eu}$  source of known activity. All data were corrected for detector efficiency. The HPGe detector was placed outside the vacuum vessel so the x-rays traveled through 3.3 mm of quartz (vacuum window) and 1.4 m of air gap before reaching the detector. Therefore x-rays of 50 keV or less energy experienced a nonlinear absorption curve with energy and were not considered in the analysis.

Following the deconvolution method prescribed by [9] an exponential function was fitted to the bremsstrahlung spectra extracting an estimate for the hot electron temperature (for a Maxwellian electron energy distribution function). Therefore, any non-Maxwellian features (non-exponentially decaying with energy) such as the peak in x-ray power that typically appears around 80-110 keV as can be seen in Fig. 2 were excluded. Fitting of the x-ray spectra for hot electron temperature began at 125 keV (see Figs. 2 and 3) for all spectra with the exception of 13 GHz operation for  $B_{min}/B_{ecr}=0.5$  (the smallest  $B_{min}$ ) where the fitting region began at 100 keV to accommodate for the overall lower energy bremsstrahlung distribution. The apparent bi-Maxwellian spectra for  $B_{min}/B_{ecr}=0.9$  in Fig. 2 had a change

Table 2: Key SuSI Parameters for Two Different Magnetic Field Configurations

Frequency	18 GHz						13 GHz					
	400 W		200 W			100 W			100 W			
Microwave Power												
$B_{min}/B_{ecr}$	0.5	0.73	0.5	0.73	0.9	0.5	0.73	0.9	0.5	0.73	0.9	
Drain Current (mA)	1.47	1.71	1.44	1.4	1.33	0.94	1.08	1.08	1.03	1.03	1.03	
Injection Pressure ( $10^{-8}$ mbar)	9.1	9.3	13	14	13	8.7	8.9	8.7	6.3	6.1	6.6	
Extraction Pressure ( $10^{-8}$ mbar)	1.5	1.6	1.9	1.9	1.8	1.6	1.3	1.6	0.94	0.74	0.92	
O <sup>6+</sup> Current ( $e\mu A$ )	59	61	35	64	68	13	30	39	4	17	21	
O <sup>4+</sup> Current ( $e\mu A$ )	64	65	81	66	71	32	60	48	42	59	47	
O <sup>2+</sup> Current ( $e\mu A$ )	75	78	83	79	63	60	73	64	73	53	43	

in slope around 300 keV, masking away this feature decreased the temperature by 4% compared to its inclusion. Effects due to bi-Maxwellian features in bremsstrahlung spectra were not accounted for in the dataset as a whole, however isolating the higher temperature component of the spectra at  $B_{min}/B_{ecr}=0.9$  in Fig. 2 by fitting from 300 keV resulted in a temperature of 67 keV which is 30% higher than that obtained from fitting at 125 keV.

X-ray power was chosen as a figure of merit of the plasma because it is weighted by the energy and photon counts. X-ray power transported through the collimation channel provides a relative measure related to electron losses because the x-ray production rate on solid targets (extraction electrode) is many orders higher than for gas targets. The total x-ray power emission was calculated by summing the x-ray power for each channel (discretized photon energy bin) of the 13 bit MCA starting at 50 keV through the end of the file at 1440 keV. The x-ray power error was calculated by taking the fractional uncertainty  $1/\sqrt{N}$  for a Poisson distribution, with  $N$  the number of detections per channel (uncorrected for detector efficiency), and weighing it by the x-ray power in that channel. Each channel x-ray power error was summed in quadrature (assumed independent and random) to generate the total x-ray power error.

## RESULTS AND DISCUSSION

The behavior of hot electron temperature with choice of low energy fitting boundary was explored for 18 GHz operation at 100 W, with the intent of estimating the electron temperature error. Figure 3 shows how the hot electron temperature changed with fitting region starting between 80-170 keV terminating at 1440 keV. A data mask that includes the non-exponentially decaying portion of the bremsstrahlung spectra (80-100 keV region) produced an artificially high hot electron temperature from the decrease in slope about the peak in bremsstrahlung power. In the case of  $B_{min}/B_{ecr}=0.9$  the temperature increases beyond 120 keV as the higher temperature but lower intensity portion of the hot electron distribution is weighted more strongly. For Figs. 4 and 9 the hot electron temperature error was generated propagating a  $\pm 10\%$  deviation in mask energy about 125 keV except for 13 GHz operation at  $B_{min}/B_{ecr}=0.5$  when the energy used was 100 keV, in accord with our previous statements. The

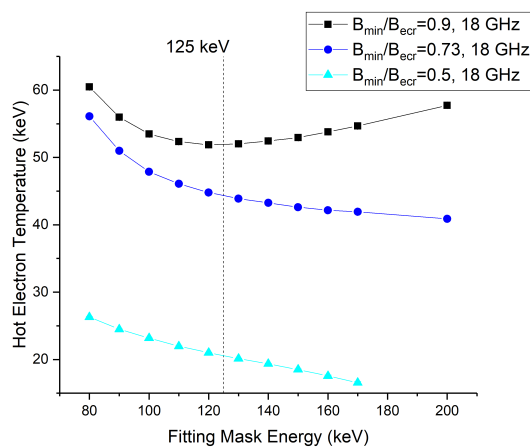


Figure 3: Hot electron temperature from fitting with an exponential decay function for different choices of the starting energy of the fitting function (fitting mask energy). The hot electron temperature changed with fitting range because the plasma generating the bremsstrahlung is not completely Maxwellian. 125 keV was selected as the mask energy to process all spectra (except 13 GHz with  $B_{min}/B_{ecr}=0.5$ ) to minimize the influence of the bremsstrahlung peak around 80-110 keV while maximizing the fitting region.

error bars in this case do not represent a 68% confidence interval but rather the deviation using three fit ranges.

The hot electron temperature (from fitting the bremsstrahlung spectra) increased with magnetic minimum as shown in Fig. 4. The trend and the absolute values of hot electron temperature with increasing  $B_{min}$  were consistent (including the rate of change) with the findings in [1], where temperature increased with the absolute value of the magnetic minimum. The two fields:  $B_{min}/B_{ecr}=0.5$  at 18 GHz and  $B_{min}/B_{ecr}=0.73$  at 13 GHz had approximately the same magnetic minimum ( $B_{min}=0.3$  T) and hot electron temperature. For  $B_{min}=0.3$  T, the extraction mirror ratio ( $B_{ext}/B_{min}$ ) was 30% lower at 13 GHz than for 18 GHz (see Table 1). Comparing 100 W cases, the x-ray power for  $B_{min}/B_{ecr}=0.73$  at 13 GHz ( $7.1\pm 0.9$  pW) was 30% higher than  $B_{min}/B_{ecr}=0.5$  at 18 GHz ( $5.3\pm 0.7$  pW) as seen in Fig. 5 suggesting the difference in x-ray power was the result of the reduced mirror ratio for 13 GHz operation.

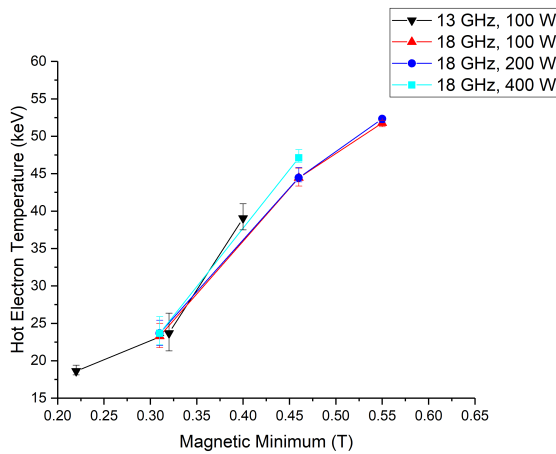


Figure 4: Hot electron temperature from fitting of the axial bremsstrahlung emission. The temperature depended on magnetic minimum independent of frequency and microwave power.

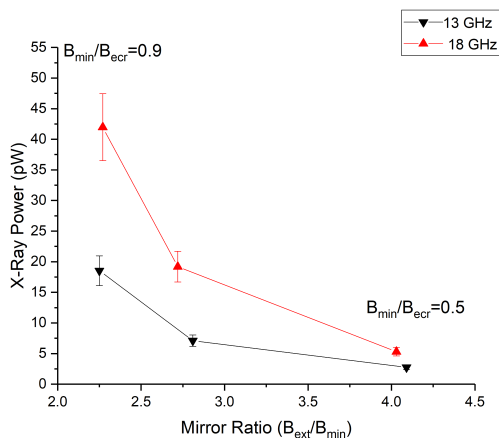


Figure 5: X-ray power with changing mirror ratio ( $B_{ext}/B_{min}$ ) for 13 GHz and 18 GHz operation with a microwave power level of 100 W.

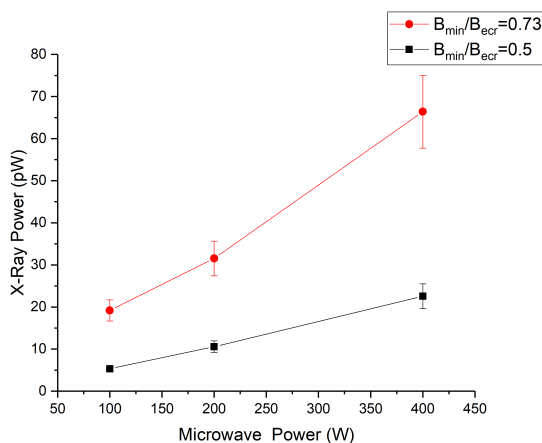


Figure 6: Total integrated x-ray power for all non-attenuated photons (greater than 50 keV) as a function of microwave power at 18 GHz. X-ray power increased linearly with microwave power.

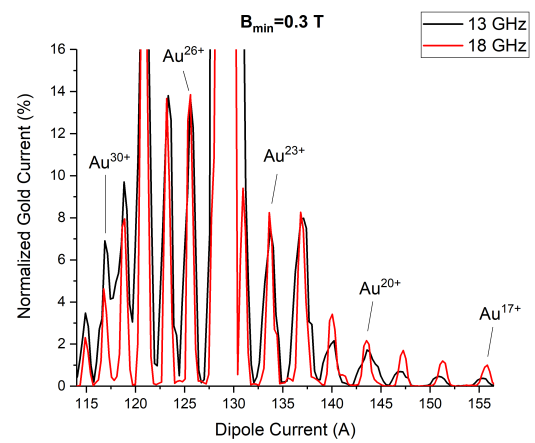


Figure 7: Gold CSD normalized to the sum of all gold currents for  $B_{min}=0.3$  T at 100 W microwave power. The total extracted current for 13 GHz operation was  $1.55 \text{ e}\mu\text{A}$  while for 18 GHz operation was  $8.80 \text{ e}\mu\text{A}$ .

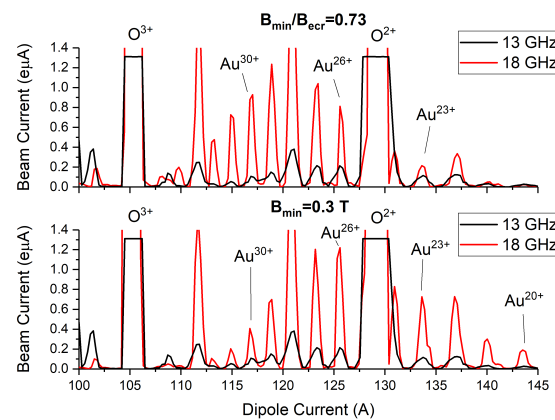


Figure 8: CSD of gold for a sputtering voltage of -500 V and with a microwave power level of 100 W. The gold currents extracted when coupling 13 GHz microwaves to drive the plasma was about an order of magnitude lower than those obtained with 18 GHz microwaves for either constant  $B_{min}$  or ECR zone size.

X-ray power increased linearly with microwave power as shown in Fig. 6. A similar relationship was observed as a dynamic heat load on the VENUS cryostat [7]. The hot electron temperature remained static with increasing power as seen in Fig. 4 so the increased power is not from a redistribution of the electrons to higher energies, instead likely the result of increasing plasma density.

Sputtering to produce highly charged ions is sensitive to the local and global plasma density: The sputtering yield (in general) depends on the ion density at the sputter sample while the ionization probability of the neutral sputtered material depends on the electron density along the path of travel through the plasma. The gold CSD's were peaked at the same charge states as seen in Fig. 7 for constant  $B_{min}$ , but the lower frequency and mirror ratio produced a slightly larger percentage of high charge states. However, the gold currents when operating at 13 GHz were nearly an order of

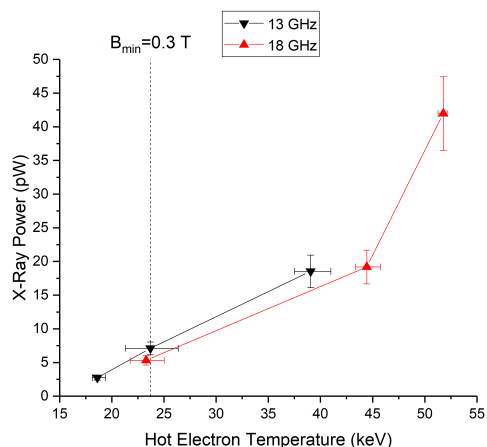


Figure 9: X-ray power as a function of hot electron temperature comparing 13 GHz and 18 GHz frequencies at 100 W microwave power for all six magnetic fields used for the study. For 13 GHz operation, x-ray power increased linearly with electron temperature for each magnetic field configuration while 18 GHz operation generated double the x-ray power for a 17% increase in temperature when changing the magnetic field from  $B_{min}/B_{ecr}=0.73$  to  $B_{min}/B_{ecr}=0.9$ .

magnitude lower than at 18 GHz as shown in Fig. 8 when controlled for microwave power, ECR zone size, and  $B_{min}$  suggesting the density was lower for 13 GHz. Higher frequency operation may pay dividends when it comes to metallic beam production even with lower magnetic fields, due to an increased plasma density for the higher frequency. Additionally, for constant mirror ratio, the x-ray power from the 18 GHz plasma was larger than that produced at 13 GHz in Fig. 5 further supporting the established idea that higher microwave frequency generates a denser plasma.

It may be possible that higher 13 GHz power levels could have been used to compensate for the reduced density when compared to 18 GHz operation. In particular, for the case of  $B_{min}=0.3$  T an additional 200 W of microwave power (microwave power level of 300 W) would be required to equalize the x-ray power for a mirror ratio of 2.8 in Fig. 5 based on the trend in Fig. 6 obtained at 18 GHz for  $B_{min}/B_{ecr}=0.5$ . The gold current increased nonlinearly with microwave power at 18 GHz for  $B_{min}=0.3$  T for charge states  $Au^{35+}$ - $Au^{30+}$ . In particular,  $Au^{30+}$  current increased by about a factor of 3 for every factor of 2 increase in microwave power, and if  $Au^{30+}$  current increased at a similar rate for 13 GHz operation the gold current at 300 W would have been about  $0.6 \mu A$  which is the same order as the measured  $Au^{30+}$  current ( $0.4 \mu A$ ) suggesting lower densities obtained with lower microwave frequencies can be compensated for with increased microwave power.

The oxygen support gas currents for 13 GHz and 18 GHz operation for 100 W were often less than a factor of two apart as seen in Table 2. The high charge state performance ( $O^{6+}$ ) was consistently better for 18 GHz operation than at 13 GHz (except for  $B_{min}=0.3$  T where 13 GHz operation slightly outperformed 18 GHz) similar to the behavior reported in [4]

comparing 18 GHz and 24 GHz performance with argon for kilowatts of microwave power.

In all plasmas studied the x-ray power increased as a function of hot electron temperature. For 13 GHz operation the x-ray power increased linearly with hot electron temperature for the three magnetic field configurations. However, for 18 GHz operation x-ray power increased sharply for  $B_{min}/B_{ecr}=0.9$  where the x-ray power doubled for only a 17% increase in electron temperature (compared to  $B_{min}/B_{ecr}=0.73$ ) as seen in Fig. 9. For comparison, the x-ray power doubled for a 80% increase in hot electron temperature between  $B_{min}/B_{ecr}=0.5$  and  $B_{min}/B_{ecr}=0.73$ . The increased x-ray power at this field and frequency combination may be the result of cyclotron instabilities, characterized in part by bursts of microwave and x-ray power in ECRIS appearing as the  $B_{min}/B_{ecr}$  ratio increases beyond around 0.7 for microwave powers as low as 50 W [2]. Cyclotron instabilities convert hot electron kinetic energy into microwave energy resulting in hot electrons escaping the magnetic bottle [10]. Cyclotron instabilities in the hotter denser 18 GHz plasma for  $B_{min}/B_{ecr}=0.9$  ( $B_{min}=0.55$  T) likely produced increased hot electron losses resulting in increased x-ray power as measured in our detector. These instabilities may have been present for 13 GHz operation but perhaps due to the lower temperature electrons for  $B_{min}/B_{ecr}=0.9$  ( $B_{min}=0.4$  T) and the lower plasma density x-ray bursts were too small in amplitude to appear within our measurement sensitivity.

## REFERENCES

- [1] J. Benitez, C. Lyneis, L. Phair, D. Todd, D. Xie, "Recent bremsstrahlung measurements from the superconducting electron cyclotron resonance ion source VENUS", in *Proc. ECRIS'16*, Busan, South Korea, 2016, paper MOCO04, pp. 23-29.
- [2] O. Tarvainen *et al.*, *Plas. Sourc. Sci. Technol.*, vol. 23, p. 025020, 2014.
- [3] P. Zavodszky *et al.*, *Rev. Sci. Instrum.*, vol. 77, p. 03A334, 2006.
- [4] G. Machicoane *et al.*, "First results at 24 GHz with the superconducting source for ions (SuSI)", in *Proc. ECRIS'14*, Nizhny Novgorod, Russia, paper MOOMMH03, pp. 1-4.
- [5] R. Geller, "Min-B ECRIS for highly charged ions", *Electron Cyclotron Resonance Ion Sources and ECR Plasmas*, IOP Publishing Ltd., Bristol and Philadelphia, 1996, pp. 394-409.
- [6] C. Lyneis, "Scaling laws in electron cyclotron resonance ion sources", in *Proc. ECRIS'16*, Busan, South Korea, 2016, paper MOCO01, pp. 1-4.
- [7] D. Leitner *et al.*, *Rev. Sci. Instrum.*, vol. 79, p. 033302, 2008.
- [8] T. Ropponen *et al.*, "Bremsstrahlung and ion beam current measurements with SuSI ECR ion source", in *Proc. ECRIS'10*, Grenoble, France, 2010, paper WECAK04, p. 171-174.
- [9] M. Lamoureux and P. Charles, *Radiation Phys. Chem.*, vol. 75, pp. 1220-1231, 2006.
- [10] S. Golubev, and A. Shalashov, *JETP Lett.*, vol. 86, pp. 91-97, 2007.